Framework for Measurement of Battery State-of-Health (Resistance) Integrating Overpotential Effects and Entropy Changes Using Energy Equilibrium

Karanjot Singh [a], Tegoeh Tjahjowidodo [b], Loïc Boulon [c], Mir Feroskhan [a,*]

[a] School of Mechanical and Aerospace Engineering, Nanyang Technological University, 50 Nanyang Avenue, Singapore 639798

[b] Department of Mechanical Engineering Technology, Jan Pieter de Nayerlaan 5, 2860 Sint-Katelijne-Waver, KU Leuven, Belgium

[c] Université du Québec à Trois Rivières, Trois Rivières, QC G8Z4M3 Québec, Canada

* Corresponding author: Tel: +65 67905580; E-mail address: mir.feroskhan@ntu.edu.sg (Mir Feroskhan)

HIGHLIGHTS

- Energy equilibrium approach is used to characterize internal resistance in a cell.
- A new reversible resistance component established based on entropy changes.
- Degradation factors associated with each resistance component for health analysis.
- The entropy changes contribute nearly 40% to overall losses at low state-of-charge.

ABSTRACT

The internal resistance of a battery represents the losses due to heat generation during energy conversion. The state-of-health is used to quantify the increase (degradation) of resistance with usage. However, the current state-of-health analysis merges the total internal resistance into one component. Consequently, the underlying cause of resistance degradation is not understood leading to incorrect estimate of battery health. Therefore, this paper presents a comprehensive framework based on energy equilibrium for the categorization and health analysis of total internal resistance. It is divided into 2 components: one based on irreversible overpotential (includes polarization) effects and a new second resistance component originated from reversible entropy changes. For $LiFePO_4$ cells used in this work, it is observed that the contribution of entropy changes (hitherto unrecognized) to the overall losses increases from $4-10\%$ to more than 40% as state-of-charge reduces. State-of-health of each component is obtained by the determination of its associated degradation factor to quantify the underlying mechanism of resistance degradation. In conclusion, the increase in irreversible resistance is primarily attributed to the permanent loss of active material. Correspondingly, the reversible resistance increase is associated to the formation of concentration gradients in the electrodes due to past load profile and ambient conditions.

KEYWORDS

State-of-Health of resistance

Resistance degradation

Energy equilibrium

Irreversible and entropy change resistance

Discharge current limitation

Lithium-ion batteries

1 Introduction

The world is rapidly moving in the direction of the utilization of electric energy as a response to the increasing energy demands. Wide variety of electrochemical batteries are used to store the electric energy for efficient usage. For their safer and reliable operation, *state-of-health* (SoH) is used to quantify the degradation of the battery performance with usage and prevent sudden failure by estimating the remaining useful life. An increase in internal resistance means the battery health has degraded which, in turn, affects its capacity and current (power) limits. There are various methods used in literature to define the SoH based on capacity fade as well as increase in internal resistance [1]. This enables the individual health analysis of both capacity fade and internal resistance with the latter being the focus of the present work.

The electric power available at the output of the battery depends on the terminal voltage which is lower than the *Open-Circuit-Voltage* (OCV) due to internal energy losses observed in the form of heat generation. The main sources of heat generation are the irreversible heat of reaction due to overpotential effects and the reversible heat of entropy [2]. For practical purposes, the losses due to heat generation are parameterized by the internal resistance which depends on the operating conditions [3]. However, the current methods categorize the steady-state total internal resistance into ohmic and polarization resistance considering the overpotential effects only (assuming entropy changes to be low) [4] as depicted in Figure 1. Nevertheless, it is shown in [5] that the contribution of the reversible heat of entropy can be comparable or even exceed the irreversible heat depending on the cell chemistry. Therefore, it is essential to analyze the impact of both irreversible and reversible effects on battery SoH to understand the underlying cause of resistance degradation. The present work aims to introduce a framework which includes the reversible entropy changes into the discrete health analysis, thus making it useful for dynamic applications.

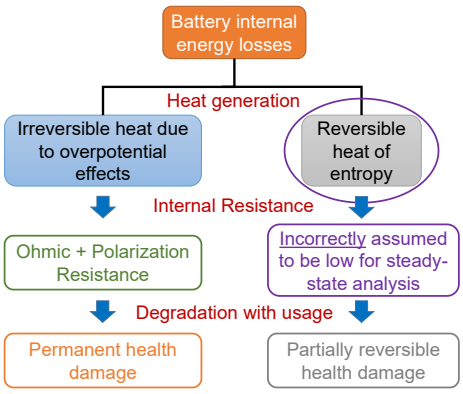

Figure 1 Categorization of energy losses in the form of internal resistance for degradation analysis.

1.1 Empirical and Mechanistic Methods for SoH Analysis

A model-based approach provides a robust way to evaluate the effect of operating conditions on the battery characteristics [6, 7]. Equivalent-circuit based models using a resistor in series with one or more parallel RC circuits (polarization circuit) have been used to characterize the dynamics of batteries [8, 9, 10, 11]. In this approach, the entropy changes are merged together with the polarization circuit and consequently, excluded in the steady-state analysis as the voltage across the capacitor stabilizes. Generally, for modelling purpose, the parameters of the equivalent circuit are identified experimentally to attain a best-fitted model. The deteriorating effect of use and ageing can then be observed in the form of capacity fade and increase in internal resistance of the cell which can be quantified by the SoH [4]. Hence, continuous parameter adaptation is essential for the control of battery operations and determining the SoH. Adaptive online models based on different variants of Kalman filter [12, 13, 14, 15], particle filter [16, 17], sliding mode observer [18], least square algorithm [19] and extreme learning machine [20] have been proposed to estimate the change in battery parameters and determine the SoH. Hence, the adaptive models take battery ageing into account with satisfactory results. However, the accuracy of the parameter adaptation is affected by the exclusion of the entropy changes in the steady-state analysis. Due to the correlation between entropy changes and *state-of-charge* (SoC), their effect on the SoH needs to be analysed discretely.

Similarly, the methods based on the analysis of differential voltage (DV) [21, 22] or incremental capacity (IC) [23, 24] curves can be used for analysing the SoH. They are useful in identifying the cause of battery health deterioration based on the changes observed in the peaks and slope of the dV/dQ (DV) or dQ/dV (IC) curves. Wang et al. [25] and Weng et al. [26] made use of the charging voltage curves to estimate the IC curves for online application. Wang et al. used centre least squares method to smoothen the voltage curves and reduce the sensitivity to noise in voltage measurement. Weng et al., on the other hand, used Support Vector Regression (SVR) to obtain the IC curves. However, voltage error accumulation over time and sensitivity to charging conditions (charging current and temperature) limits the online application of this method. The sample entropy of a characteristic associated with the cell performance: discharge voltage [27, 28] and charging temperature [29], has also been used for SoH estimation. However, they require a large amount of dataset for data fitting and parameter estimation. The accuracy of the method is also dependent on relevant feature selection (charging profile, resting time, discharge voltage etc.). Furthermore, the parameters used in the analysis are also not physically interpretable to understand the reasons for battery health deterioration.

1.2 Framework based on Energy Equilibrium for Determining SoH (Resistance)

As discussed in Section 1.1, the methodology used to predict the battery SoH should be able to address the deteriorating effect of the reversible entropy changes in an isolated manner. These reversible effects are a direct result of constantly changing operating conditions, dynamic power requirements and past load profile. Therefore, the framework presented in this paper aims to quantify the degradation mechanism: irreversible overpotential effects and reversible entropy changes, using physically interpretable degradation factors. With the primary focus on the determination of SoH of resistance, the contribution of this work is two folds:

- Since we are dealing with the energy losses, the resistance degradation is categorized into two components derived from the fundamental energy equilibrium approach. This results in the inclusion of the hitherto excluded entropy changes in addition to the irreversible overpotential effects (including polarization) during the stead-state analysis. The degradation factor associated with each resistance component helps to quantify the SoH of resistance and the underlying mechanism of degradation.
- The dynamic discharge current limits are computed using the measured resistance degradation factors. This helps determine the dynamic power limits during battery operation so that it stays within the defined voltage limits.

The work in this paper is organized as follows. The theoretical foundation for categorizing the total internal resistance into irreversible (overpotential effects) and reversible (entropy) components with their respective degradation factors is discussed in Section 2. The experimental procedure used to determine the parameters based on temperature, current and SoC is described in Section 3. The experimental procedure used to validate the method and determine the degradation factors is described in Section 4. The drawn conclusions and future work are discussed in Section 5.

2 Battery Parameters Derived from Energy Equilibrium Approach

During the battery operation, the measurement of voltage provides the foundation for most of the methods discussed for analyzing the battery health. However, the measurement is generally affected by long-term as well as recent power charge/discharge history. The OCV of an electrochemical cell is representative of the maximum electrical energy that can be derived from it. The difference between OCV and the measured terminal voltage is representative of the overall energy losses. Therefore, at any given instant, a general energy balance [30] can be used to account for the difference between the OCV and the measured cell voltage (terminal voltage). The primary forms of energy loss in the cells are irreversible resistive dissipation (overpotential voltage drop characterized by ohmic and polarization resistance of the cells) and reversible entropy losses; assuming energy losses due to chemical reactions and heat of mixing to be low. The proposed methodology uses the energy equilibrium approach to represent the voltage change due to each type of loss by a resistance component. Consequently, a new approach is introduced to categorize the internal resistance into two components and determine the SoH of resistance using the degradation factors associated with each resistance component. Hence, the effect of reversible entropy changes, which is well studied in the thermal analysis of the battery [2, 31] but ignored in the steady-state battery parameter determination, can be taken into account.

2.1 Resistance Degradation Analysis using Energy Equilibrium

The chemical energy stored in the cell is delivered in the form of useful electric work obtained from the terminal voltage and discharge current. The heat generated during this conversion accounts for the energy loss. Assuming the heat of formation due to chemical reactions to be low and neglecting the effect of heat of mixing [2, 32], the rate of heat generation follows the following relationship:

$$\frac{dQ_{gen}}{dt} = I\,[V_{term} - V_{OCV}(SoC, T_{cell})] = I\,[V_{cell} - V_{OCV}(SoC, T_{cell})] + I\,T_{cell}\,\frac{\partial V_{OCV}(SoC, T_{cell})}{\partial T_{cell}} \quad \textbf{(1)}$$

where, V_{term} is the terminal voltage of the cell, V_{OCV} is the open-circuit voltage of the cell, T_{cell} is the cell temperature, $V_{cell} = V_{term} - T_{cell}\frac{\partial V_{OCV}}{\partial T_{cell}}$ is the cell potential specifically accounting for irreversible overpotential effects.

Hence, the power loss due to heat generation comprises of the loss due to the irreversible overpotential effects (including polarization) and the reversible potential change (entropy change). Overpotential effects that originate from the heat generated by the irreversible internal resistance is always exothermic leading to a loss of energy. The reversible potential change can be either positive or negative based on the entropy change. Using resistance to represent the potential changes in equation (1), the total resistance measured at any instant consists of an irreversible and a reversible component:

$$R_{ti}(I, SoC, T_{cell}) = R_{irr}(I, SoC, T_{cell}) - \frac{T_{cell}}{I}\,\frac{\partial V_{OCV}(SoC, T_{cell})}{\partial T_{cell}} \quad \textbf{(2)}$$

where, $R_{irr} = \frac{(V_{OCV} - V_{cell})}{I}$ is the irreversible component of internal resistance at a given SoC and $R_{ti} = \frac{(V_{OCV} - V_{term})}{I}$ is the total internal resistance. The second component of the resistance, $R_{ent} = -\frac{T_{cell}}{I}\,\frac{\partial V_{OCV}(SoC, T_{cell})}{\partial T_{cell}}$ is derived from the entropy change. Considering the degradation of both irreversible and reversible components, actual resistance at any given instant is represented as:

$$R_{act\,ti}(I, SoC, T_{cell}) = \theta_{irr}\,R_{base\,irr}(I, SoC, T_{cell}) + \theta_{rev}\,R_{base\,ent}(I, SoC, T_{cell});$$

$$\theta_{irr} = \frac{R_{act\,irr}}{R_{base\,irr}}, \qquad \theta_{rev} = \frac{R_{act\,ent}}{R_{base\,ent}} \quad \textbf{(3)}$$

where, $R_{act\,ti}$, $R_{act\,irr}$ and $R_{act\,ent}$ are the actual/present total resistance, irreversible resistance and entropy change resistance measured at a given SoC and cell temperature respectively, θ_{irr} and θ_{rev} are the degradation factors of the irreversible and reversible components of internal resistance respectively, $R_{base\,irr} = R_{ti} - R_{base\,ent}$ and $R_{base\,ent} = -\frac{T_{cell}}{I}\,\frac{\partial V_{OCV}}{\partial T_{cell}}$ are the irreversible and reversible components of resistance respectively used as the baseline values for degradation comparison (preferably, measured when the cell is new).

The normalized degradation factors defined in this work allow the use of energy balance equation for general dynamic problems. The factor θ_{rev} accounts for the change in entropy due to spatial changes in lithium concentration. Therefore, it is representative of the battery conditions at the time of measurement which includes temperature and discharge current history. While θ_{irr} accounts for the irreversible increase in resistance due to the formation of side products. Considering the normalization, a value greater than 1 means the resistance has increased compared to the reference values which depicts resistance degradation. Therefore, the approach enables the identification and quantification of the degradation mechanism based on the degradation factors. A higher θ_{rev} indicates greater concentration gradients leading to entropy

changes while an increase in θ_{irr} depicts irreversible increase in the internal resistance due to side reactions. Considering the resistance degradation of the battery in steady-state (as irreversible resistance includes both electrical and polarization resistance), the equivalent circuit used for battery performance analysis is illustrated in Figure 2.

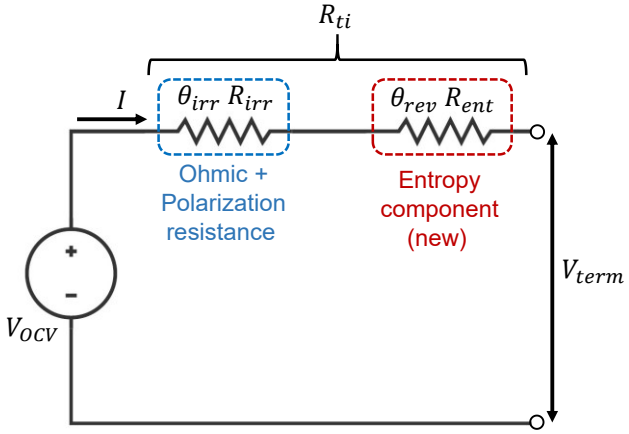

Figure 2 Steady-state equivalent circuit for resistance degradation analysis.

2.2 Remodelled SoH of Resistance

Since the degradation due to entropy changes (concentration gradients) is partially reversible, it is affected by the recent current profile and ambient conditions. However, the irreversible component does not vary significantly with changing conditions. Therefore, it provides a relevant factor to normalise $R_{act\ ti}$ and determine the actual *state-of-health of resistance* (SoH_R). Hence, we remodel the SoH_R using equation (3) as follows:

$$SoH_R = \frac{R_{act\ ti}}{R_{base\ irr}} = \theta_{irr} + \theta_{rev}\ r_{ent-irr}(I, SoC, T_{cell}) \quad \textbf{(4)}$$

where, $r_{ent-irr} = \frac{R_{base\ ent}}{R_{base\ irr}}$ is the ratio of the baseline values of the reversible and irreversible components of resistance. It can be observed that $r_{ent-irr}$ is directly proportional to $\frac{\partial V_{OCV}(SoC,T_{cell})}{\partial T_{cell}}$ which is a function of SoC in the given temperature range. As $r_{ent-irr}$ changes sign with $\frac{\partial V_{OCV}(SoC,T_{cell})}{\partial T_{cell}}$, the factor θ_{rev} may increase or decrease the magnitude of SoH_R. This remodelled definition of SoH_R differs from the existing approach in use where it is defined as the ratio of actual and baseline total resistance $\left(\frac{R_{act\ ti}}{R_{base\ ti}}\right)$. The proposed method helps overcome the limitations of the existing approach (refer Section 4.1 for details).

2.3 Discharge Current Limitation

The resistance degradation directly affects the capacity and power available in a battery as it is a complex electrochemical device which is allowed to function within a *safe operating area* (SOA). SOA of a particular battery is defined based on the minimum (cut-off voltage) and maximum voltage limits in order to avoid rapid deterioration and failure. As such, the discharge current that can be drawn from the battery is dependent on the instantaneous internal resistance. It is limited

either by an absolute maximum discharge current (battery parameter based on cell chemistry) or a dynamically decreasing discharge limit, whichever is lower, to keep the battery within SOA. Since the terminal voltage should be more than the minimum voltage ($V_{cut-off}$), the dynamic discharge current limit based on voltage limits, $I_{lim\,volt}$ is obtained by substituting $R_{ti} = V_{OCV} - V_{cut-off}$ [33], and accounting for θ_{irr} and θ_{rev} factors into equation (2):

$$I_{lim\,volt} = \frac{V_{OCV} - V_{cut-off} + \theta_{rev}\, T_{cell}\, \frac{\partial V_{OCV}}{\partial T_{cell}}}{\theta_{irr}\, R_{irr}}; \quad \textbf{(5)}$$

$$V_{cut-off} = 2.5\ V \text{ for LiFePO}_4 \text{ cells}$$

The absolute discharge current limit and power limit are subsequently defined as follows:

$$I_{lim} = \min\left[I_{lim\,cap}, I_{lim\,volt}\right]; P_{lim} = V_{term}\, I_{lim} \quad \textbf{(6)}$$

where, $I_{lim\,cap}$ is the maximum discharge limit suggested by the cell manufacturer as per the cell chemistry. Correlating the discharge current limit (I_{lim}) with SoC estimation provides a measure of the capacity available for that current under the given conditions. It can be observed in equation (5) that an increase in the irreversible resistance (higher θ_{irr}) leads to a given discharge limit being attained at higher SoCs and hence, loss of capacity. Therefore, it can be concluded from this analysis that the capacity available during the battery operation is affected by a change in the internal resistance.

3 Baseline Parameter Identification

The experimental tests for the baseline battery parameter identification have been carried out on modules of commercially available $LiFePO_4$ cells with a nominal capacity of 20 Ah. The operating voltage of the cells is between 2.5 V and 3.65 V with a maximum pulse discharge current of 200 A (10C). These tests are conducted using Chroma 17020 regenerative battery module test system with Wewontech TH-408 environmental chamber (Figure 3) for ambient temperature control. Pulse discharge and charge tests as suggested in [9, 34] are applied to identify R_{ti}, R_{ent} and R_{irr} as functions of the temperature, SoC and current. Five battery modules consisting of three cells each are used for the tests. The steady-state equivalent circuit parameters (Figure 2) are thus obtained from the average of parameters calculated from the three cells of a module, in order to account for manufacturing inconsistencies [35]. Before the actual measurements, each module is passed through three cycles of standard charge/discharge as suggested by the manufacturer, to make their behavior stable for measurement.

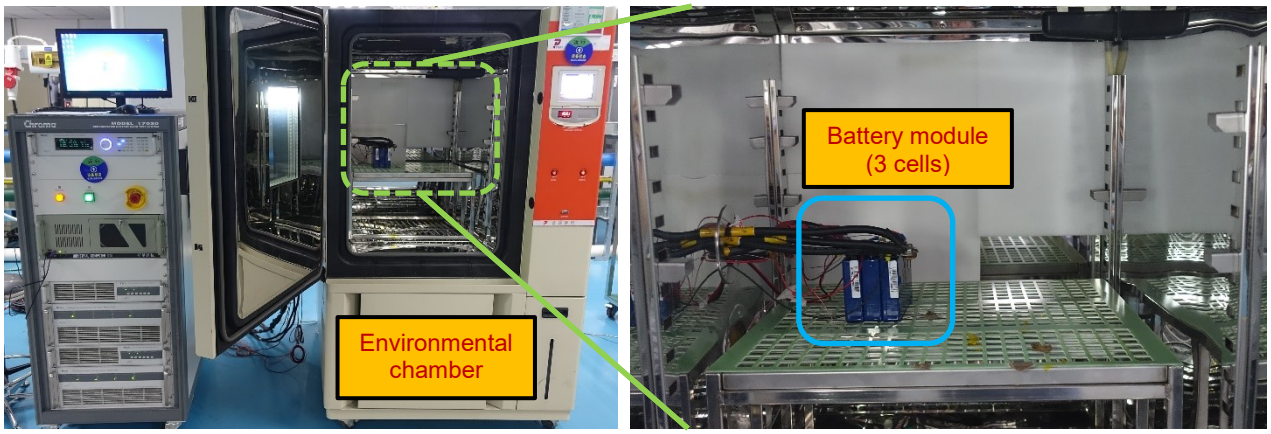

Figure 3 Test setup for battery parameters identification.

Furthermore, the tests have been conducted to obtain the baseline parameters covering the complete discharge current range (up to $10\ C$) at the temperatures of 10°C and 25°C. Since the measurement of total internal resistance includes the losses due to polarization, the length of the selected discharge pulse should be sufficient to allow the polarization effects to stabilize. Hence, a discharge pulse spanning 2 Ah for approximately 10% SoC discharge (approximately, as the actual nominal capacity is found during the tests) is selected for the tests. The ambient temperature and resting period between consecutive pulses (as listed in Table 1) are established based on the lumped parameter thermal model. The goal is to achieve the end of pulse temperatures of approximately 10°C and 25°C, respectively, during each test for effective measurements. Every discharge test is preceded by charging each cell of the battery module independently at the standard temperature of 25°C. Constant current charging up to 3.65 V at a constant current of 10 A (~0.5C) is followed by a constant voltage charging at 3.65 V until the current dropped to 1 A (~0.05C). This is followed by rest at the required test temperature for 2 hours to achieve thermal equilibrium. The test is terminated when one of the cells reaches the cut-off voltage of 2.5 V as lower voltage levels might lead to irreversible capacity loss (as suggested by the manufacturer). Total discharge obtained from the cells until cut-off voltage is used to obtain the capacity available at different currents and temperatures.

Discharge current (A)	Ambient temperature (°C)		Rest period between consecutive pulses (min.)
	10°C testing	25°C testing	
$2\ (0.1C)$	10	25	10
$20\ (1C)$	8	23	10
$60\ (3C)$	6	22	15
$100\ (5C)$	5	21	25
$140\ (7C)$	5	21	35
$200\ (10C)$	4	20	45

Table 1 Test conditions used for parameter identification using pulse discharge.

3.1 OCV and Entropy Change Plots

Initially, the determination of OCV at the temperatures of 10°C and 25°C is performed by discharging the battery module at the nominal current of 20 A (~1C). Discharge pulses spanning 2 Ah are applied to the battery module with each pulse followed by a rest period of 2 hours to allow the cells to reach steady-state (stable voltage output). OCV is taken as the

measured voltage level at the end of the rest period. Hence, the OCV is determined as a function of SoC at the required temperatures. The entropy change $\left(\frac{\partial V_{OCV}(SoC,T_{cell})}{\partial T_{cell}}\right)$ is then computed (illustrated in Figure 7a) using the OCV values obtained at the temperatures of 10°C and 25°C. ∂V_{OCV} is the difference of OCV values obtained at 25°C and 10°C respectively and ∂T_{cell} is the temperature difference.

3.2 Determination of Resistance Components

The total internal resistance (R_{ti}) is determined as a function of SoC for each of the discharge currents (2 A to 200 A) mentioned in Table 1. Essentially, it characterizes the total voltage recovery after the load is removed. Figure 4 illustrates an example of the dynamic voltage response of a cell for a discharge pulse of 2 Ah at an applied current of 60 A. The terminal voltage measured at the end of a discharge pulse ($V_{term\,end}$) represents the total voltage drop at a given SoC. While OCV represents the steady-state voltage at the given SoC measured at the instant just before the beginning of the discharge pulse. Hence, R_{ti} is obtained as a function of SoC using the following equation:

$$R_{ti}(SoC) = \frac{V_{OCV}(SoC) - V_{term\,end}}{I} \quad \textbf{(7)}$$

R_{ent} is also calculated as a function of SoC for different discharge currents and is essentially obtained by scaling the entropy change $\left(\frac{\partial V_{OCV}(SoC,T_{cell})}{\partial T_{cell}}\right)$ with the term $\frac{T_{cell}}{I}$:

$$R_{ent}(SoC) = -\frac{T_{cell}}{I}\frac{\partial V_{OCV}(SoC,T_{cell})}{\partial T_{cell}} \quad \textbf{(8)}$$

Notably R_{ent} changes sign (“crossover” point) as the entropy change becomes negative (Figure 7a). R_{irr} is then evaluated by rearranging equation (2) as follows:

$$R_{irr}(SoC) = R_{ti}(SoC) - \left[-\frac{T_{cell}}{I}\frac{\partial V_{OCV}(SoC,T_{cell})}{\partial T_{cell}}\right] = R_{ti}(SoC) - R_{ent}(SoC) \quad \textbf{(9)}$$

R_{ti}, R_{ent} and R_{irr} obtained at 10°C and 25°C are presented in Figure 5. Nominal capacity of 21.11 Ah (obtained by discharging the cells at nominal conditions of 2 A current at 25°C) is used to calculate the SoC. Resistances for each current value are plotted to the exhaustion of capacity (one of the cells in the module reaching terminal voltage of 2.5 V) at that particular discharge current.

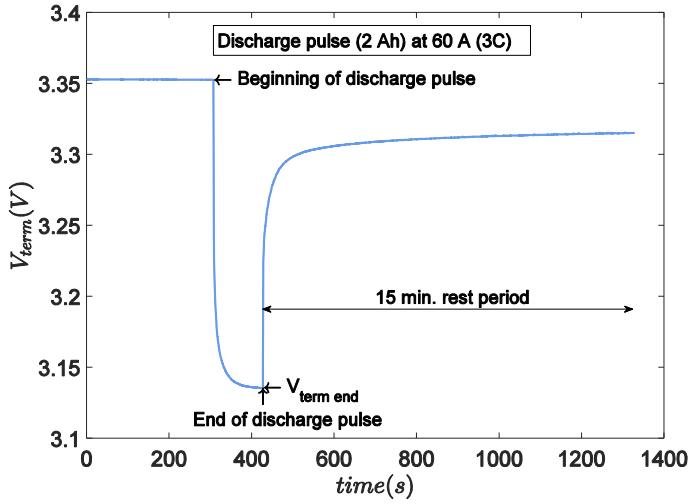

Figure 4 Voltage response at 60 A for a discharge pulse (2 Ah) used for determination of resistance components.

R_{ent} is computed up to the current used to define the nominal capacity (0.1C), 2 A in the present test case, to keep it finite, since it is inversely proportional to the current. It is also observed in Figure 5h that R_{irr} becomes negative at smaller values of current for a small range of SoC before it turns to positive again. This anomalous behaviour could be explained by the additional time available for the polarization at low currents while the entropy of the system is reducing (negative entropy change) till the end of the two phase transition. Two phase transition is reported to end near SoC of approximately 0.05 [36, 37] after which R_{ti} and R_{irr} increase rapidly. The MATLAB code for generating the plots can be found at [38].

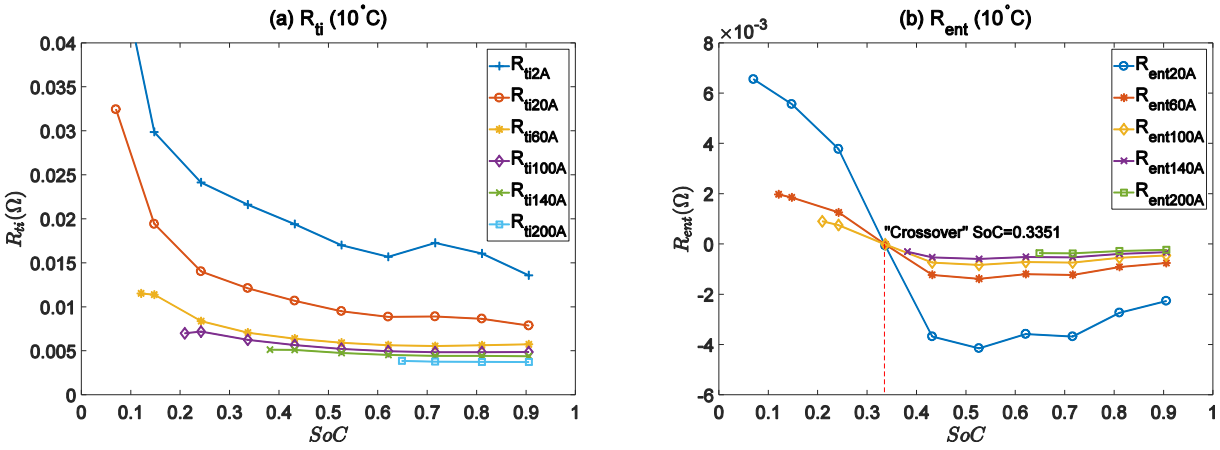

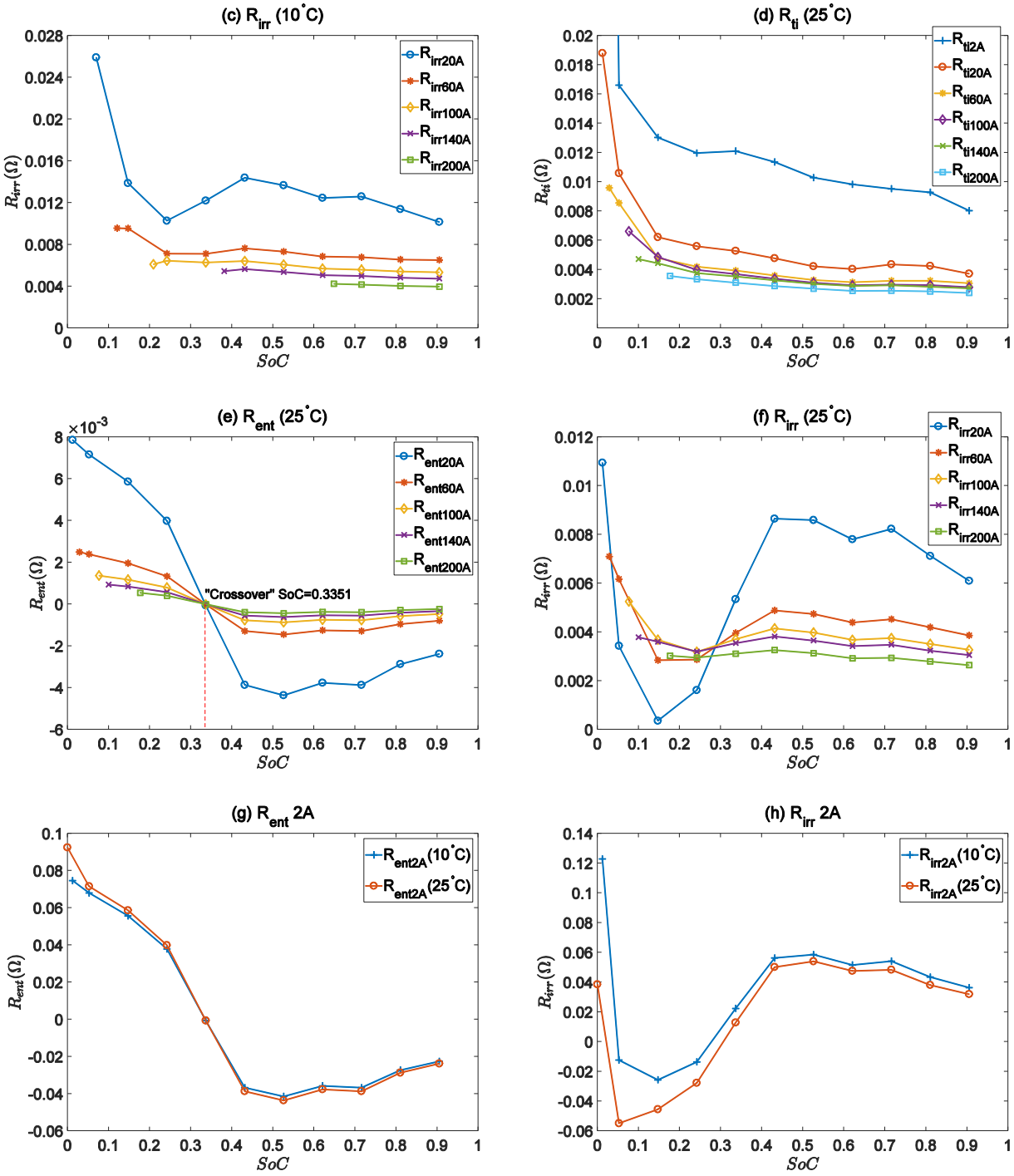

Figure 5 Resistance plots as functions of SoC at different values of current at 10°C and 25°C, a) $\boldsymbol{R_{ti}}$ at 10°C *, b) $\boldsymbol{R_{ent}}$ at 10°C, c) $\boldsymbol{R_{irr}}$ at 10°C, d) $\boldsymbol{R_{ti}}$ at 25°C *, e) $\boldsymbol{R_{ent}}$ at 25°C, f) $\boldsymbol{R_{irr}}$ at 25°C, g) $\boldsymbol{R_{ent}}$ for nominal capacity discharge current (0.1C), h) $\boldsymbol{R_{irr}}$ for nominal capacity discharge current (0.1C).

*Note- Plots are enlarged to amplify the effect of resistance variation at higher discharge currents.

3.3 Capacity Determination using Discharge Current Limits

The capacity available for a specified discharge current under the given ambient conditions is determined by discharging the cells at that current up to the cut-off voltage (2.5 V for $LiFePO_4$ cells). Correspondingly, the nominal capacity (indicative of total charge available) is taken as the maximum capacity extracted experimentally for a discharge of 0.1C (2 A for our case) at 25°C. However, the capacity reduces with resistance degradation as the cut-off voltage is reached earlier due to

an increase in resistance. The framework introduced in this work helps in the estimation of the capacity available with resistance degradation.

The SoC at which a given discharge current limit is reached (indicative of capacity available at that current) can be obtained by substituting the corresponding R_{irr} (function of temperature and SoC for given current) into equation (5). Figure 6a illustrates the evolution of the experimental discharge current limits obtained during the baseline parameter identification testing in Section 3. Subsequently, the plots in Figure 6b and Figure 6c are obtained by plotting the right hand side of equation (5) for the baseline R_{irr} values ($\theta_{irr} = \theta_{rev} = 1$). They illustrate the advancement of discharge current limits at 10°C and 25°C respectively. For example, the capacity limit for 200 A discharge is obtained experimentally at the SoC of 0.6494 at 10°C. Substituting the corresponding values of R_{irr} for 200 A into equation (5), the progression of discharge current limit is illustrated in Figure 6b. Eventually, the discharge current limit of approximately 201 A is obtained at the experimentally determined SoC limit of 0.6494. Correspondingly, the advancement of current limits for 140A, 100A, 60A, 20A and 2A is also illustrated in Figure 6b and Figure 6c. The marginal difference in the current limits at the expected discharge capacity is obtained due to the test termination criterion used. The criterion resulted in discharge being stopped whenever one of the three cells in a module reached the cut-off voltage of 2.5 V. The cells are expected to reach the cut-off voltage almost simultaneously as they are charged individually. However, as mentioned in Section 3, the average of the resistances of the three cells in a module is used for the calculation of discharge current limits to account for cell manufacturing inconsistencies. Therefore, it might be a good idea to use the highest cell resistance for this calculation in order to ensure safe operation. The application and validation of this method with resistance degradation is demonstrated in Section 4.4.

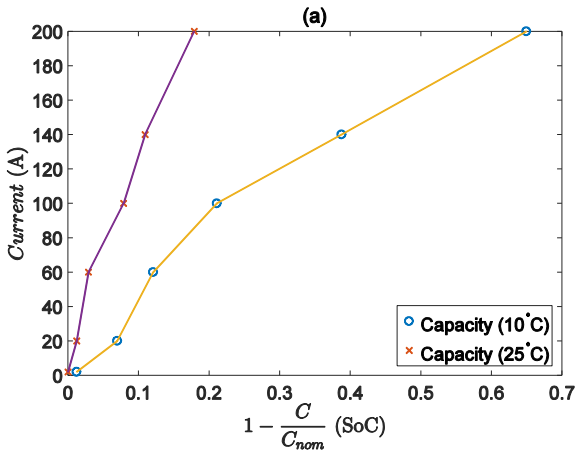

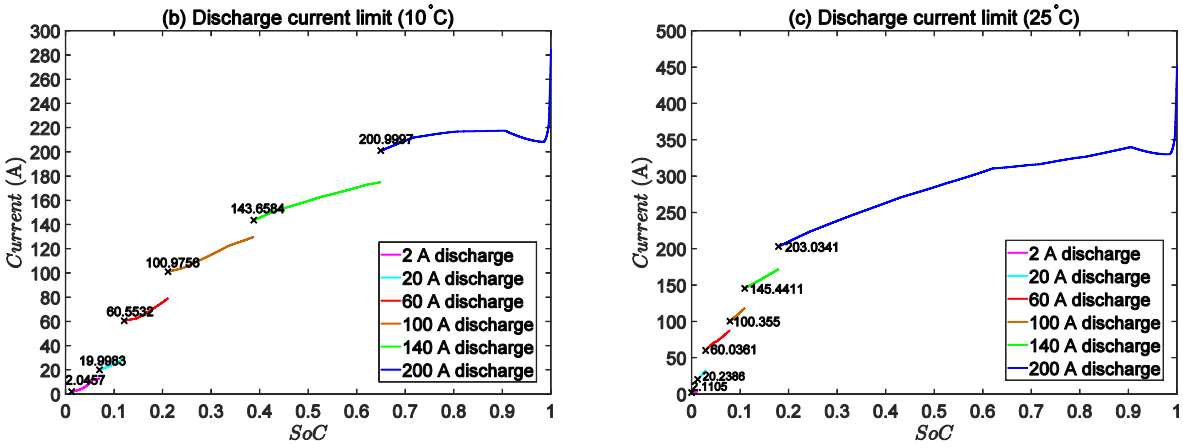

Figure 6 Capacity plots at 10°C and 25°C, a) Capacity obtained at different values of current experimentally, b) Discharge current limits for obtaining capacity available at 10°C, c) Discharge current limits for obtaining capacity available at 25°C.

4 Experimental Validation Testing and Analysis

The tests for the validation of the proposed resistance degradation methodology is conducted on two battery modules. They are initially discharged for 30 cycles at different currents in order to simulate accelerated battery ageing. Subsequently, the battery modules are subjected to customized tests using the same testing equipment as presented in Section 3. The testing is conducted at 10°C since higher and distinctive values of resistance are observed at that temperature (see Figure 5) which would aid in observing the resistance degradation distinctly for different currents. As explained in Section 3, each cell in the two modules is charged independently using the standard procedure of a constant current followed by a constant voltage charging at 25°C. This is followed by resting at the test temperature of 10°C for 2 hours to achieve thermal equilibrium. The discharge cycle sequence consisted of discharge at a given current in pulses of 2 Ah (repeated until the capacity limit is reached at that current level) under the conditions specified in Table 1. The discharge is stopped before 2 Ah pulse ended if one of the cells in the module reached the cut-off voltage (i.e., capacity at the given discharge current is exceeded). The discharge procedure started with 200 A (10C) discharge current (maximum discharge current suggested by the cell manufacturer), followed successively by decreasing currents of 140 A, 100 A, 60 A, 20 A and 2 A on both modules. The module is rested for 1 hour after capacity exhaustion at each discharge current before moving to the subsequent current level.

4.1 Limitations of Existing SoH (Resistance) Measurement

Using the existing approach, the SoH of resistance used for estimating the resistance degradation is expressed as [33, 39, 1]:

$$SoH_R^{old} = \frac{R_{act\ ti}}{R_{base\ ti}} \tag{10}$$

However, this approach merges the entropy changes with the overpotential effects and is therefore, not useful for determining the contribution of each component to the overall resistance degradation. The entropy change plot based on

the measurement of $\frac{\partial V_{OCV}}{\partial T_{cell}}$ at the temperatures of 10°C and 25°C is derived as per the procedure discussed in Section 3.1 and depicted in Figure 7a. It is found to change signs from positive to negative at the SoC of 0.3351 followed by an increased in magnitude. This change of sign and magnitude impacts the measurement of the resistance degradation significantly as the contribution of the entropy changes to the overall losses increases. It is observed in Figure 7b that the SoH of resistance obtained using equation (10) is nearly constant for the SoC ranging from 0.40 to 0.85, while it increases below the SoC of 0.3351 (when entropy changes its sign). This observation can be explained by analysing the factors affecting the measurement of total internal resistance using equation (2). During the measurement of the actual total resistance $R_{act\ ti}$, the actual capacity of the cell is lower than the nominal capacity observed during the measurement of base total resistance $R_{base\ ti}$ due to ageing and usage. However, the nominal capacity is still used for SoC calculation and comparison with the baseline resistance values. As a result of the reduced capacity, the actual SoC is lower than the calculated SoC. Hence, there is a shift to lower SoC along the entropy change curve (refer Figure 7a) for the measured actual reversible resistance component $R_{act\ ent}$.

During the testing, the discharge currents for SoC greater than 0.40 ranged from 100 A to 200 A as seen in Figure 8a, Figure 8b. The factor $\frac{T_{cell}}{I}$ is relatively low in magnitude for high discharge currents which reduces the contribution of $R_{act\ ent}$ in the magnitude of $R_{act\ ti}$ compared to the contribution of the actual irreversible resistance component $R_{act\ irr}$. It is also observed that the entropy changes at a slow rate in the SoC range of approximately 0.40 to 0.98 as illustrated in Figure 7a. Consequently, an incremental shift in entropy along the entropy change curve in this SoC range does not have a sizeable impact on the value of $R_{act\ ti}$, if the factor $\frac{T_{cell}}{I}$ is comparable for successive measurements. However, it is observed that $R_{act\ ti}$ increases rapidly below the SoC at which $R_{act\ ent}$ becomes positive (i.e., $\frac{\partial V_{OCV}}{\partial T_{cell}}$ turns negative) as observed in Figure 7b. This results from an increase in the contribution of the reversible component $R_{act\ ent}$ to the total resistance $R_{act\ ti}$, relative to the contribution of the irreversible component $R_{act\ irr}$. Consequently, SoH_R^{old} increases at a rapid rate below the SoC at which the contribution of reversible entropy changes increases, as per equations (2) and (10). Therefore, the existing definition of the SoH of resistance merges together the contribution of the reversible and the irreversible components to the overall resistance degradation. Since the irreversible degradation is permanent while the reversible degradation is partially or fully reversible, it is essential to separately analyze the contribution of each component to the resistance degradation. In the electrochemical cells which demonstrate rapid entropy changes over the entire span of the battery charge, the contribution of the reversible component would be significantly higher and clearly observed throughout the discharge. Hence, the existing method used to determine the SoH of resistance is not useful for understanding the actual cause of degradation.

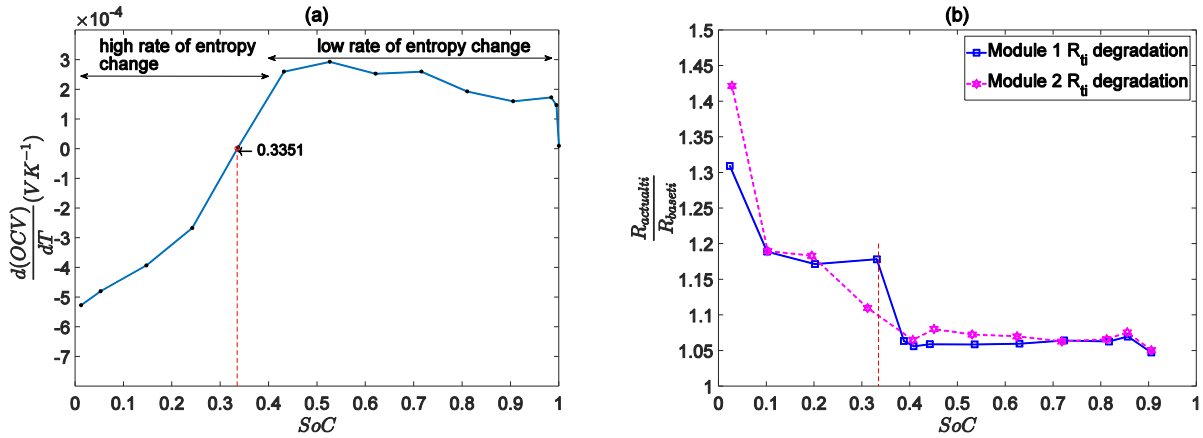

Figure 7 a) Entropy change plot and b) $\boldsymbol{SoH_R^{old}}$ as function of SoC.

4.2 Measurement of Proposed SoH

In order to truly analyze the instantaneous effect of resistance degradation, it is imperative that the measured actual total resistance is normalized with respect to a component which does not change significantly with SoC. Therefore, the proposed definition of SoH (refer Section 2.1) compares the actual total resistance with the baseline irreversible resistance instead of the baseline total resistance. Consequently, SoH_R provides an indication of the overall increase in the instantaneous total resistance compared to the irreversible component of resistance. The points of measurement at the end of discharge pulse for the validation tests on the two modules are shown on entropy change plots in Figure 8a, Figure 8b. It can be observed in Figure 8c that the SoH_R increases at low SoCs as the contribution of the reversible component $R_{act\ ent}$ increases. Furthermore, the framework helps quantify the contribution of each resistance component to the overall resistance degradation using their associated degradation factors as discussed in Section 4.3. Hence, it overcomes the limitations of the existing approach for detecting the degradation mechanism as discussed in Section 4.1.

4.3 Recommended Method for Determination of Degradation Factors

After the successful determination of the SoH_R as discussed in Section 4.2, the factors θ_{irr} and θ_{rev} can further help understand the underlying cause for the resistance degradation. The suggested method to determine the degradation factors is discussed as follows:

I. Determine the SoH_R while recording the current and SoC at the end of the discharge pulse.

II. For the two different measurements of SoH_R, determine the factor $r_{ent-irr}$ for each measurement.

III. Consequently, the two unknown degradation factors, θ_{irr} and θ_{rev} are determined using equation (4).

In the present illustration, the SoH_R determined for 200 A at SoC of 0.8561 (point 2 in Figure 8a) is taken as the constant first measurement. The degradation factors are then determined corresponding to the respective SoC values of the second measurement. Therefore, the SoH_R determined for the corresponding discharge currents at the decreasing SoC values are used as the variable second measurement. Similarly, SoH_R for 200 A at SoC of 0.8553 (point 2 in Figure 8b) is used

as the first measurement for calculating θ_{irr} of module 2. The degradation factors thus determined are demonstrated in Table 2. The results using SoH_R determined at 140A, 100 A and 60 A as the first measurement points with SoH_R for respective lower discharge currents as the second measurement points demonstrate similar values and trend (for details, refer Table 4 in Appendix A). For the present analysis, the focus is kept on the irreversible degradation factor θ_{irr} as illustrated in Figure 8d. The irreversible degradation, an indicator of a permanent increase in resistance, is observed to increase with discharge. This can be attributed to the use of high discharge currents at the beginning of discharge which leads to increased electrode stresses. The degradation values are observed to be relatively stable in the SoC range of approximately 0.10 to 0.30 which coincides with the discharge currents of 3C (60 A) and 1C (20 A). The irreversible resistance degradation then increases marginally at the lower discharge current (2 A) as the lithium ions have more time to engage in side reactions leading to increased *solid-electrolyte interface* (SEI) growth.

Remark: Entropy $\left(\frac{\partial V_{OCV}}{\partial T_{cell}}\right)$ changes at a slow rate in the high SoC range of approximately 0.40 to 0.98 (see Figure 7a), demonstrating absolute values of the order of 1e-4. This makes the solution of equation (4) to be sensitive to the precision of $r_{ent-irr}$ and SoH_R. To overcome this limitation, the inherent scaling factor in the entropy change resistance: $\frac{T_{cell}}{I}$ can be exploited. By solving equation (4) for $r_{ent-irr}$ and SoH_R obtained at different currents, the effect of the factor $\frac{T_{cell}}{I}$ is amplified. Additionally, the resistance varies significantly for each discharge current (refer Figure 5). Therefore, higher current ratios of the two measurements used for determining the degradation factors lead to more accurate results. The precision constraint can also be avoided by utilizing the measurements taken in the SoC range where the entropy is changing rapidly (SoC range of approximately 0.05 to 0.40 as seen in Figure 7a). Therefore, this improved approach offers an accurate method for estimating the degradation of each resistance component through the entire range of the battery operation.

Current span	Nominal SoC	θ_{irrdeg} Module 1	θ_{revdeg} Module 1
$200-140$	$0.8561-0.7231$	1.0762	1.1762
$200-140$	$0.8561-0.6294$	1.0830	1.2881
$200-140$	$0.8561-0.5356$	1.0818	1.2679
$200-140$	$0.8561-0.4419$	1.0867	1.3480
$200-140$	$0.8561-0.4081$	1.1073	1.6858
$200-100$	$0.8561-0.2963$	1.0882	1.3722
$200-60$	$0.8561-0.2017$	1.0990	1.5500
$200-20$	$0.8561-0.1015$	1.0961	1.5031
$200-2$	$0.8561-0.0234$	1.0997	1.5621
Current span	Nominal SoC	θ_{irrdeg} Module 2	θ_{revdeg} Module 2
$200-140$	$0.8553-0.7183$	1.0915	1.3347
$200-140$	$0.8553-0.6246$	1.0831	1.1976
$200-140$	$0.8553-0.5308$	1.0790	1.1304
$200-140$	$0.8553-0.4509$	1.0688	0.9627
$200-140$	$0.8553-0.4065$	1.1071	1.5909
$200-100$	$0.8553-0.3119$	1.0989	1.4562
$200-60$	$0.8553-0.1951$	1.1065	1.5817
$200-20$	$0.8553-0.1031$	1.1008	1.4883
$200-2$	$0.8553-0.0282$	1.1153	1.7260

Table 2 Irreversible and reversible degradation factor values for current spans starting from 200 A.

4.4 Discharge Current Limits

Besides explaining the cause of resistance degradation, the degradation factors can further be used for the determination of the dynamic discharge current limit as discussed in Section 3.3. Theoretically, it is determined by substituting the measured values of the factors θ_{irr} and θ_{rev} in equation (5) as presented in Table 3. The current limits are depicted as a function of SoC for both the tested battery modules in Figure 9a and Figure 9b. Subsequently, by correlating the discharge current limit to the SoC, it is observed that about 1.6% and 1.1% nominal capacity reduction is observed in the modules 1 and 2 respectively owing to the increased *IR* losses. The accuracy of the discharge current limits is improved by considering the highest cell resistance instead of the average of resistance of the cells in a module (as mentioned in Section 3.3). Consequently, the maximum error between the theoretical and true (observed) discharge current limits is restricted to a maximum of 3.7% as illustrated in Figure 9d. The contribution of entropy changes on the voltage drop in equation (5) is expressed as $\Delta V_{ent} = \theta_{rev}\, T_{cell}\, \frac{\partial V_{OCV}}{\partial T_{cell}}$. It can be observed in Figure 9c that their contribution increases as the dynamic discharge current limit reduces. This trend is correlated to the fact that the magnitude of entropy increases with decreasing SoC as observed in Figure 7a.

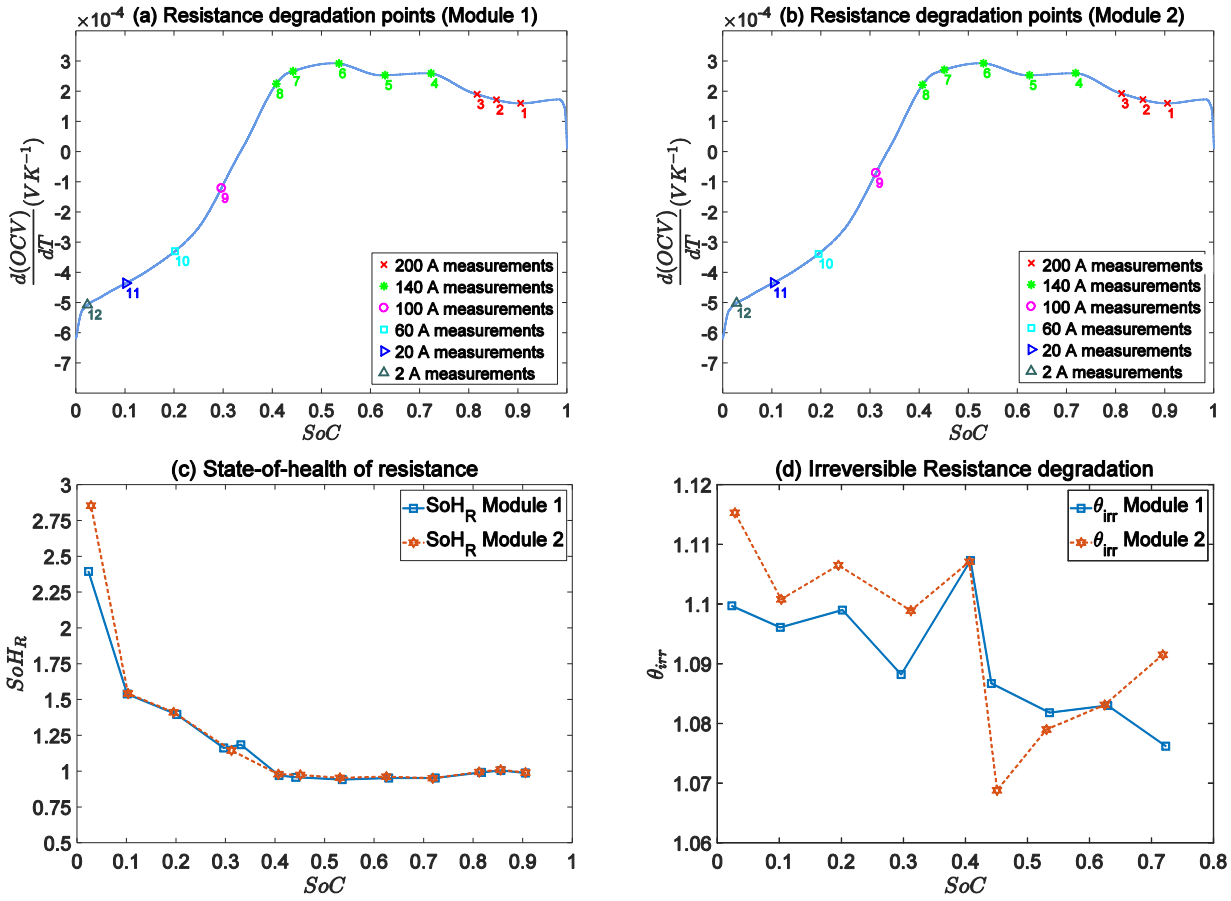

Figure 8 Resistance degradation measurement, a) Module 1 measurement points on entropy plot, b) Module 2 measurement points on entropy plot, c) SoH of resistance, and d) Irreversible resistance degradation factor as functions of SoC.

Remark: $LiFePO_4$ cells used in the current work have a flattened entropy change curve with a low magnitude in the SoC range of $40\ \%$ to $100\ \%$. Therefore, the contribution of entropy changes to the overall voltage drop is relatively low in this range. However, other cell chemistries might have a larger contribution at higher dynamic current limits and SoCs based on their entropy change characteristics. This makes the proposed resistance degradation framework universally useful for different cell chemistries.

True discharge current limit measured experimentally ($I_{true\ lim}$) (A)	Theoretical current limits (A)			
	Module 1		Module 2	
	Including entropy changes	Excluding entropy changes	Including entropy changes	Excluding entropy changes
20	19.74	28.23	20.59	28.86
60	61.44	78.98	61.04	77.44
100	97.84	105.19	101.96	106.35
140	134.80	120.48	137.46	127.01
200	195.69	177.18	195.80	183.75

Table 3 A comparison of the theoretical current limits obtained with experimental observations.
Note- The limits computed "including entropy changes" are the actual theoretical limits. Meanwhile, the limits calculated "excluding entropy changes" are used to determine the contribution of the entropy changes to the overall voltage drop.

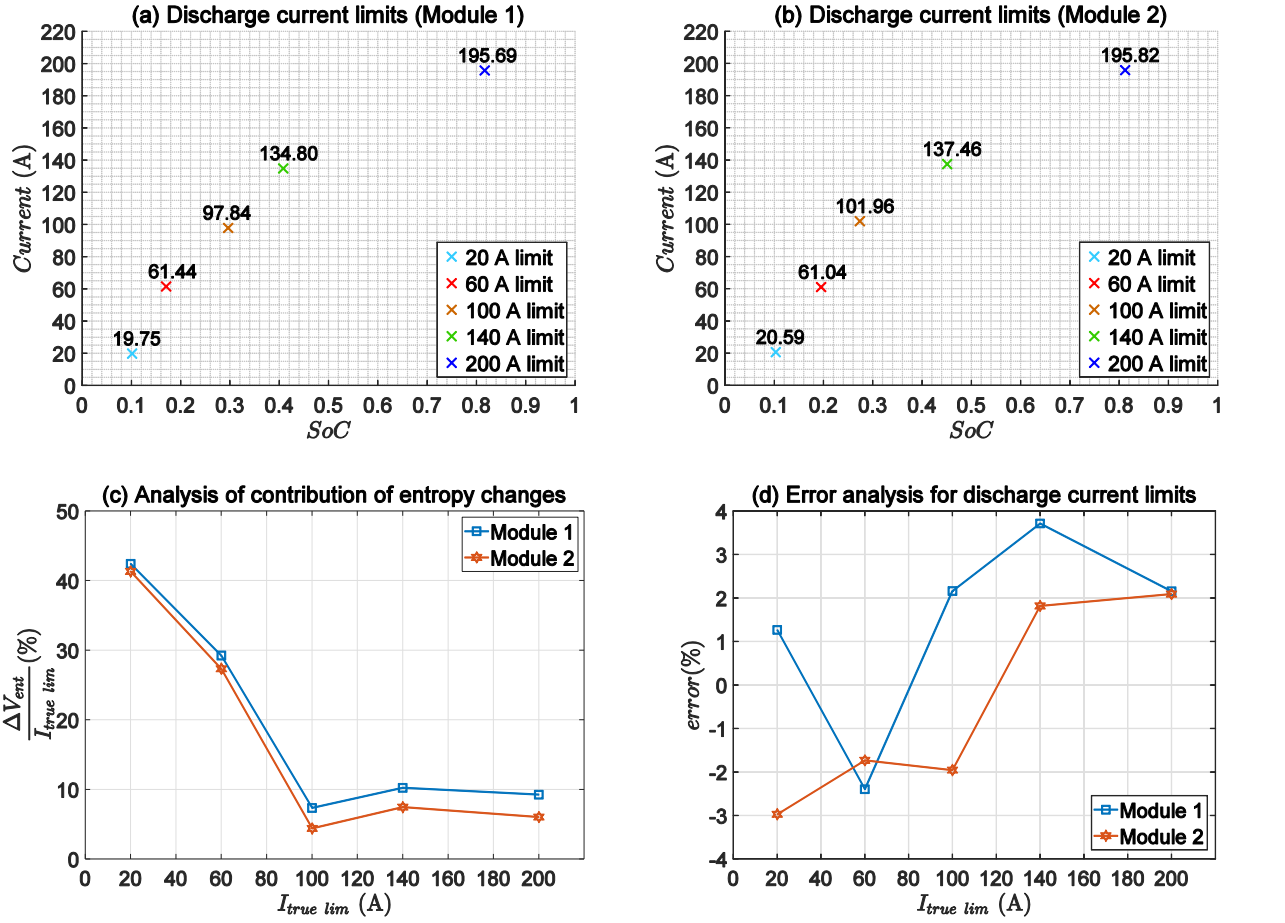

Figure 9 Validation testing: (a) Discharge current limits for Module 1, (b) Discharge current limits for Module 1, (c) percentage contribution of the entropy changes to voltage drop at true (observed) current limits, and (d) error analysis between theoretical and true (observed) current limits.

5 Conclusions and Future Work

In this study, a new approach to analyze the state-of-health of resistance is introduced. The total internal resistance is composed of the reversible resistance due to entropy change and the irreversible resistance due to overpotential effects. It is demonstrated that the degradation of both resistance components needs to be evaluated individually to understand the underlying cause of overall resistance degradation. It can be inferred from the analysis that the increase in resistance originating from the growth of SEI and side products is primarily observed in the irreversible resistance degradation. Whereas, the reversible resistance degradation is mainly attributed to the concentration gradients of lithium ions and their effect on the entropy. The main outcomes of the proposed resistance degradation method are summarized as follows:

- Resistance degradation is divided into two types, i.e., irreversible (overpotential effects) and the reversible (entropy change) degradation component.
- A remodeled definition of the SoH of resistance is presented which provides a better measure for analyzing the instantaneous increase in resistance making it more suitable for dynamic applications.
- Irreversible resistance degradation is observed to be independent of SoC. In accordance with the experimental results, it is deduced that the degradation factor θ_{irr} increases gradually for high discharge currents (additional mechanical stress on the electrodes) as well as low discharge currents (increased side reactions).
- Reversible resistance degradation is shown to be a function of SoC. The degradation factor θ_{rev} varies with the slope of entropy change. The entropy changes are partially reversible and are able to account for the dynamic effects of the recent load profile and ambient conditions on the battery performance.

Furthermore, the capacity loss covering increased IR losses can be predicted with the knowledge of the degradation factors. The resistance components with their respective degradation factors are used to find the discharge current limits as a function of SoC and therefore, determine the discharge capacity available at the applied current.

As a future work, it is hypothesized that the reversible degradation might be useful in predicting the capacity fade due to the loss of lithium and active material to SEI formation. Since the entropy change is a function of SoC, the reversible degradation factor estimates the scale of deviation in the entropy change compared to the base entropy change measurement. Accurate determination of the entropy change in the given temperature range would be the foundation for this approach. Subsequently, the framework discussed in this paper can be shown capable of estimating the battery performance deterioration due to ageing considering both the increased internal resistance and capacity fade.

Appendix A

The irreversible and reversible degradation values obtained for different discharge currents.

Current span	Nominal SoC	θ_{irrdeg} Module 1	θ_{revdeg} Module 1
$140-100$	$0.4081-0.2963$	1.0856	1.4197
$140-60$	$0.4081-0.2017$	1.0970	1.5602
$100-60$	$0.2963-0.2017$	1.0705	1.6986
$140-20$	$0.4081-0.1015$	1.0932	1.5131
$100-20$	$0.2963-0.1015$	1.0777	1.5657
$60-20$	$0.2017-0.1015$	1.1300	1.3881
$140-2$	$0.4081-0.0234$	1.0974	1.5648
$100-2$	$0.2963-0.0234$	1.0764	1.5902
$60-2$	$0.2017-0.0234$	1.0958	1.5668
Current span	Nominal SoC	θ_{irrdeg} Module 2	θ_{revdeg} Module 2
$140-100$	$0.4065-0.3119$	1.0981	1.4793
$140-60$	$0.4065-0.1951$	1.1064	1.5823
$100-60$	$0.3119-0.1951$	1.0926	1.6539
$140-20$	$0.4065-0.1031$	1.0993	1.4935
$100-20$	$0.3119-0.1031$	1.0975	1.4995
$60-20$	$0.1951-0.1031$	1.1682	1.2613
$140-2$	$0.4065-0.0282$	1.1177	1.7236
$100-2$	$0.3119-0.0282$	1.0895	1.7516
$60-2$	$0.1951-0.0282$	1.0701	1.7710

Table 4 Irreversible and reversible degradation factor values spanning different discharge currents.

Mathematical Notations

V_{OCV} Open-circuit voltage (V)

V_{cell} cell potential accounting for irreversible overpotential effects (V)

V_{term} terminal voltage (V)

$V_{cut-off}$ minimum terminal voltage allowed during discharge (V)

C current rate relative to nominal cell capacity (A)

C_{nom} nominal cell capacity (Ah)

I total discharge current (A)

$I_{lim\ volt}$ discharge current limit based on voltage (A)

$I_{lim\ cap}$ discharge current limit based on cell capability and chemistry (A)

$I_{dischg\ lim}$ absolute discharge current limit at given state (A)

Q_{gen} heat generated due to enthalpy and entropy changes (J)

R_{ent} resistance component due to entropy change (Ω)

R_{irr} resistance due to overpotential voltage drop (Ω)

R_{ti} total internal resistance (Ω)

$R_{act\ ti}$ total internal resistance measured at present state (Ω)

$SoH_{R_{ti}}^{old}$ existing definition to determine SoH of resistance

$SoH_{R_{ti}}$ new proposed definition to determine SoH of resistance

T_{cell} temperature of cell (K)

$\theta_{irr\ deg}$ degradation factor of irreversible resistance

$\theta_{rev\ deg}$ degradation factor of resistance due to entropy change

$r_{ent-irr}$ ratio of entropy change resistance and irreversible resistance

Acronyms

BMS Battery Management System

SEI Solid-electrolyte interface

$LiFePO_4$ Lithium iron phosphate

SoC state-of-charge

SoH state-of-health

OCV Open-Circuit-Voltage

SOA Safe operating area

Acknowledgement

The research conducted in this paper is funded jointly by ABB Pte Ltd, Singapore and Maritime and Port Authority (MPA) of Singapore. The authors thank Civil Aviation Authority of Singapore (CAAS) and the Air Traffic Management Research Institute (ATMRI), Singapore for their support. The authors would also like to acknowledge the support provided by Dr. Sreetej Lakkam and Mr. Govind Gour during the review process.

6 References

[1] A. Farmann, W. Waag, A. Marongiu and D. U. Sauer, “Critical review of on-board capacity estimation techniques for lithium-ion batteries in electric and hybrid electric vehicles,” *Journal of Power Sources,* vol. 281, pp. 114-130, 2015.

[2] C. Forgez, D. Vinh Do, G. Friedrich, M. Morcrette and C. Delacourt, “Thermal modeling of a cylindrical LiFePO4/graphite lithium-ion battery,” *Journal of Power Sources,* vol. 195, no. 9, p. 2961–2968, 2010.

[3] W. Waag, C. Fleischer and D. U. Sauer, “Critical review of the methods for monitoring of lithium-ion batteries in electric and hybrid vehicles,” *Journal of Power Sources,* vol. 258, pp. 321-339, 2014.

[4] M. Berecibar, I. Gandiaga, I. Villarreal, N. Omar, J. V. Mierlo and P. V. d. Bossche, “Critical review of state of health estimation methods of Li-ion batteries for real applications,” *Renewable and Sustainable Energy Reviews,* vol. 56, pp. 572-587, 2016.

[5] V. V. Viswanathan, D. Choi, D. Wang, W. Xu, S. Towne, R. E. Williford, J.-G. Zhang, J. Liu and Z. Yang, “Effect of entropy change of lithium intercalation in cathodes and anodes on Li-ion battery thermal management,” *Journal of Power Sources,* vol. 195, no. 11, pp. 3720-3729, 2010.

[6] Ewert Energy Systems, Inc, “Orion 2 BMS Operation Manual,” [Online]. Available: https://www.orionbms.com/manuals/pdf/orionbms2_operational_manual.pdf. [Accessed 15 January 2021].

[7] Y. Cui, P. Zuo, C. Du, Y. Gao, J. Yang, X. Cheng, Y. Ma and G. Yin, “State of health diagnosis model for lithium ion batteries based on real-time impedance and open circuit voltage parameters identification method,” *Energy,* vol. 144, pp. 647-656, 2018.

[8] M. A. Roscher and D. U. Sauer, “Dynamic electric behavior and open-circuit-voltage modeling of LiFePO4-based lithium ion secondary batteries,” *Journal of Power Sources,* vol. 196, no. 1, pp. 331-336, 2011.

[9] S. Abu-Sharkh and D. Doerffel, “Rapid test and non-linear model characterisation of solid-state lithium-ion batteries,” *Journal of Power Sources,* vol. 130, no. 1-2, p. 266–274, 2004.

[10] H. He, X. Zhang, R. Xiong, Y. Xu and H. Guo, “Online model-based estimation of state-of-charge and open-circuit voltage of lithium-ion batteries in electric vehicles,” *Energy,* vol. 39, no. 1, pp. 310-318, 2012.

[11] B. Xia, C. Chen, Y. Tian, M. Wang, W. Sun and Z. Xu, “State of charge estimation of lithium-ion batteries based on an improved parameter identification method,” *Energy,* vol. 90, pp. 1426-1434, 2015.

[12] G. L. Plett, “Extended Kalman filtering for battery management systems of LiPB-based HEV battery packs Part 3. State and parameter estimation,” *Journal of Power Sources,* vol. 134, no. 2, p. 277–292, 2004.

[13] F. Sun, X. Hu, Y. Zou and S. Li, “Adaptive unscented Kalman filtering for state of charge estimation of a lithium-ion battery for electric vehicles,” *Energy,* vol. 36, no. 5, pp. 3531-3540, 2011.

[14] G. Pérez, M. Garmendia, J. F. Reynaud, J. Crego and U. Viscarret, “Enhanced closed loop State of Charge estimator for lithium-ion batteries based on Extended Kalman Filter,” *Applied Energy,* vol. 155, pp. 834-845, 2015.

[15] L. Pei, C. Zhu, T. Wang, R. Lu and C. Chan, “Online peak power prediction based on a parameter and state estimator for lithium-ion batteries in electric vehicles,” *Energy,* vol. 66, pp. 766-778, 2014.

[16] S. Schwunk, N. Armbruster, S. Straub, J. Kehl and M. Vetter, “Particle filter for state of charge and state of health estimation for lithium-iron phosphate batteries,” *Journal of Power Sources,* vol. 239, pp. 705-710, 2013.

[17] J. Li, L. Wang, C. Lyu, L. Zhang and H. Wang, “Discharge capacity estimation for Li-ion batteries based on particle filter under multi-operating conditions,” *Energy,* vol. 86, pp. 638-648, 2015.

[18] I.-S. Kim, “A Technique for Estimating the State of Health of Lithium Batteries Through a Dual-Sliding-Mode Observer,” *IEEE Transactions on Power Electronics,* vol. 25, no. 4, pp. 1013 - 1022, 2010.

[19] R. Xiong, F. Sun, H. He and T. D. Nguyen, “A data-driven adaptive state of charge and power capability joint estimator of lithium-ion polymer battery used in electric vehicles,” *Energy,* vol. 63, pp. 295-308, 2013.

[20] H. Pan , Z. Lü , H. Wang, H. Wei and L. Chen, “Novel battery state-of-health online estimation method using multiple health indicators and an extreme learning machine,” *Energy,* vol. 160, pp. 466-477, 2018.

[21] I. Bloom, A. N. Jansen, D. P. Abraham, J. Knuth, S. A. Jones, V. S. Battaglia and G. L. Henriksen, “Differential voltage analyses of high-power, lithium-ion cells: 1. Technique and application,” *Journal of Power Sources,* vol. 139, no. 1-2, pp. 295-303, 2005.

[22] L. Zheng, J. Zhu, D. Dah-Chuan Lu, G. Wang and T. He, “Incremental capacity analysis and differential voltage analysis based state of charge and capacity estimation for lithium-ion batteries,” *Energy,* vol. 150, pp. 759-769, 2018.

[23] M. Dubarry, V. Svoboda, R. Hwu and B. Y. Liaw, “Incremental Capacity Analysis and Close-to-Equilibrium OCV Measurements to Quantify Capacity Fade in Commercial Rechargeable Lithium Batteries,” *Electrochemical and Solid-State Letters,* vol. 9, no. 10, pp. A454-A457, 2006.

[24] M. Dubarry, C. Truchot and B. Y. Liaw, “Synthesize battery degradation modes via a diagnostic and prognostic model,” *Journal of Power Sources,* vol. 219, pp. 204-216, 2012.

[25] L. Wang, C. Pan, L. Liu, Y. Cheng and X. Zhao, “On-board state of health estimation of LiFePO4 battery pack through differential voltage analysis,” *Applied Energy,* vol. 168, pp. 465-472, 2016.

[26] C. Weng, Y. Cui, J. Sun and H. Peng, “On-board state of health monitoring of lithium-ion batteries using incremental capacity analysis with support vector regression,” *Journal of Power Sources,* vol. 235, pp. 36-44, 2013.

[27] A. Widodo, M.-C. Shim, W. Caesarendra and B.-S. Yang, “Intelligent prognostics for battery health monitoring based on sample entropy,” *Expert Systems with Applications,* vol. 38, no. 9, pp. 11763-11769, 2011.

[28] X. Hu, S. E. Li, Z. Jia and B. Egardt, “Enhanced sample entropy-based health management of Li-ion battery for electrified vehicles,” *Energy,* vol. 64, pp. 953-960, 2014.

[29] J. Li, C. Lyu, L. Wang, L. Zhang and C. Li, “Remaining capacity estimation of Li-ion batteries based on temperature sample entropy and particle filter,” *Journal of Power Sources,* vol. 268, pp. 895-903, 2014.

[30] D. Bernardi, E. Pawlikowski and J. Newman, “A General Energy Balance for Battery Systems,” *Journal of the Electrochemical Society,* vol. 132, no. 1, pp. 5-12, 1985.

[31] K. Takano, Y. Saito, K. Kanari, K. Nozaki, K. Kato, A. Negishi and T. Kato, “Entropy change in lithium ion cells on charge and discharge,” *Journal of Applied Electrochemistry,* vol. 32, no. 3, p. 251–258, 2002.

[32] K. E. Thomas and J. Newman, “Thermal Modeling of Porous Insertion Electrodes,” *Journal of The Electrochemical Society,* vol. 150, no. 2, pp. A176-A192, 2003.

[33] A. Paryani , “Determining battery DC impedance”. Patent US8965721B2, 24 February 2015.

[34] B. Schweighofer, K. M. Raab and G. Brasseur, “Modeling of High Power Automotive Batteries by the Use of an Automated Test System,” *IEEE Transactions on Instrumentation and Measurement,* vol. 52, no. 4, pp. 1087-1091, 2003.

[35] C. Zhang, G. Cheng, Q. Ju, W. Zhang, J. Jiang and L. Zhang, “Study on Battery Pack Consistency Evolutions during Electric Vehicle Operation with Statistical Method,” in *Energy Procedia*, 2017.

[36] M. A. Roscher, J. Vetter and D. U. Sauer, “Cathode material influence on the power capability and utilizable capacity of next generation lithium-ion batteries,” *Journal of Power Sources,* vol. 195, no. 12, pp. 3922-3927, 2010.

[37] V. Srinivasan and J. Newman, “Discharge Model for the Lithium Iron-Phosphate Electrode,” *Journal of The Electrochemical Society,* vol. 151, no. 10, pp. 1517-1529, 2004.

[38] K. Singh, “Replication data for: Battery Resistance Degradation Framework validation,” 2019. [Online]. Available: https://doi.org/10.21979/N9/QJWIV9.

[39] J. M. Alvarez, M. Sachenbacher, D. Ostermeier, H. J. Stadlbauer, U. Hummitzsch and A. Alexeev, “Electric Vehicle Enhanced Range, Lifetime And Safety Through INGenious battery management,” Everlasting, February 2017.